Seasonal fluxes of carbonyl sulfide in a midlatitude forest

Róisín Commane[a,b,1], Laura K. Meredith[c,2], Ian T. Baker[d], Joseph A. Berry[e], J. William Munger[a,b], Stephen A. Montzka[f], Pamela H. Templer[g], Stephanie M. Juice[g], Mark S. Zahniser[h], and Steven C. Wofsy[a,b]

[a]Harvard School of Engineering and Applied Sciences, Harvard University, Cambridge, MA 02138; [b]Department of Earth and Planetary Sciences, Harvard University, Cambridge, MA 02138; [c]Department of Earth, Atmospheric & Planetary Sciences, Massachusetts Institute of Technology, Cambridge, MA 02139; [d]Department of Atmospheric Science, Colorado State University, Fort Collins, CO 80523; [e]Department of Global Ecology, Carnegie Institution, Stanford, CA 94305; [f]Global Monitoring Division, Earth System Research Laboratory, National Oceanic and Atmospheric Administration, Boulder, CO 80305; [g]Department of Biology, Boston University, Boston, MA 02215; and [h]Center for Atmospheric and Environmental Chemistry, Aerodyne Research Inc., Billerica, MA 01821

Edited by Graham D. Farquhar, Australian National University, Canberra, ACT, Australia, and approved October 9, 2015 (received for review February 27, 2015)

Carbonyl sulfide (OCS), the most abundant sulfur gas in the atmosphere, has a summer minimum associated with uptake by vegetation and soils, closely correlated with CO_2. We report the first direct measurements to our knowledge of the ecosystem flux of OCS throughout an annual cycle, at a mixed temperate forest. The forest took up OCS during most of the growing season with an overall uptake of 1.36 ± 0.01 mol OCS per ha (43.5 ± 0.5 g S per ha, 95% confidence intervals) for the year. Daytime fluxes accounted for 72% of total uptake. Both soils and incompletely closed stomata in the canopy contributed to nighttime fluxes. Unexpected net OCS emission occurred during the warmest weeks in summer. Many requirements necessary to use fluxes of OCS as a simple estimate of photosynthesis were not met because OCS fluxes did not have a constant relationship with photosynthesis throughout an entire day or over the entire year. However, OCS fluxes provide a direct measure of ecosystem-scale stomatal conductance and mesophyll function, without relying on measures of soil evaporation or leaf temperature, and reveal previously unseen heterogeneity of forest canopy processes. Observations of OCS flux provide powerful, independent means to test and refine land surface and carbon cycle models at the ecosystem scale.

carbonyl sulfide | carbon cycle | sulfur cycle | stomatal conductance

Carbonyl sulfide (OCS) is the most abundant sulfur gas in the atmosphere (1), and biogeochemical cycling of OCS affects both the stratosphere and the troposphere. The tropospheric OCS mixing ratio is between 300 and 550 parts per trillion (ppt) (1) (10^{-12} mol OCS per mol dry air), decreasing sharply with altitude in the stratosphere (2). In times of low volcanic activity, the sulfur budget and aerosol loading of the stratosphere are largely controlled by transport and photooxidation of OCS from the troposphere (3). The processes regulating emission and uptake of OCS are thus important factors in determining how changes in climate and land cover may affect the stratospheric sulfate layer.

Oceans are the dominant source of atmospheric OCS (4), with smaller emissions from anthropogenic and terrestrial sources, such as wetlands and anoxic soils (e.g., refs. 5 and 6) and oxic soils during times of heat or drought stress (e.g., refs. 7 and 8). The terrestrial biosphere is the largest sink for OCS (1, 4, 9, 10) with uptake by both oxic soils (e.g., ref. 11) and vegetation (e.g., ref. 9). Once OCS molecules pass through the stomata of leaves, the uptake rate of OCS is controlled by reaction with carbonic anhydrase (CA) within the mesophyll, to produce H_2S and CO_2. CA is the same enzyme that hydrolyzes carbon dioxide (CO_2) in the first chemical step of photosynthesis (12).

Studies considering the large-scale atmospheric variability of OCS have linked OCS fluxes and the photosynthetic uptake of CO_2 for regional and global scales (1, 4, 13). Leaf-scale studies have confirmed the OCS link to photosynthesis (14, 15). Initial OCS ecosystem flux estimations were made using flask sampling followed by analysis via gas chromatography–mass spectrometry (GC-MS) (13, 16), but these studies did not have sufficient resolution to examine daily or hourly controls on the OCS flux. Laser spectrometers have been developed (17, 18) to enable direct, in situ measurement of OCS fluxes by eddy covariance, and measurements of OCS ecosystem fluxes have been reported, for periods of up to a few weeks, above arid forests (19) and an agricultural field (8, 20).

Net carbon exchange in terrestrial ecosystems [net ecosystem exchange (NEE)] can be measured by eddy flux methods. NEE may be regarded as the sum of two gross fluxes: gross ecosystem productivity (GEP) and ecosystem respiration (R_{eco}). GEP is the light-dependent part of NEE, estimated by subtracting daytime ecosystem respiration (R_{eco}), computed by extrapolation of the temperature dependence of nighttime NEE (NEE – R_{eco} = GEP) (e.g., refs. 21–24). At night, NEE includes all autotrophic and heterotrophic respiration processes. During the day, GEP approximates the carboxylation rate minus photorespiration at the ecosystem scale (25). Extrapolation of nighttime R_{eco} introduces major uncertainty in the interpretation of GEP, which could be reduced, and the ecological significance of GEP increased, by developing independent methods of measuring rates of photosynthetic processes. As shown below, fluxes of OCS give more

Significance

The flux of carbonyl sulfide (OCS) provides a quantitative, independent measure of biospheric activity, especially stomatal conductance and carbon uptake, at the ecosystem scale. We describe the factors controlling the hourly, daily, and seasonal fluxes of OCS based on 1 year of observations in a forest ecosystem. Vegetation dominated uptake of OCS, with daytime fluxes accounting for 72% of the total uptake for the year. Nighttime fluxes had contributions from both incompletely closed stomata and soils. Net OCS emission was observed at high temperature in summer. Diurnal and seasonal variations in OCS flux show variable stoichiometry relative to photosynthetic uptake of CO_2. An effective model framework is shown, using an explicit representation of ecosystem processing of OCS.

Author contributions: R.C., M.S.Z., and S.C.W. designed research; R.C. and L.K.M. performed research; I.T.B., J.A.B., J.W.M., S.A.M., P.H.T., and S.M.J. contributed new reagents/analytic tools; R.C. analyzed data; and R.C., L.K.M., I.T.B., J.A.B., J.W.M., S.A.M., P.H.T., S.M.J., M.S.Z., and S.C.W. wrote the paper.

The authors declare no conflict of interest.

This article is a PNAS Direct Submission.

Data deposition: The data have been deposited in the Harvard Forest Data Archive, harvardforest.fas.harvard.edu:8080/exist/apps/datasets/showData.html?id=hf214.

[1]To whom correspondence should be addressed. Email: rcommane@seas.harvard.edu.

[2]Present address: Stanford School of Earth, Energy & Environmental Sciences, Stanford University, Stanford, CA 94305.

This article contains supporting information online at www.pnas.org/lookup/suppl/doi:10.1073/pnas.1504131112/-/DCSupplemental.

direct information on one of the major controls on GEP, stomatal conductance, rather than GEP itself, providing a powerful means for testing and improving ecosystem models and for scaling up leaf-level processes to the whole ecosystem.

Here we describe the factors controlling the hourly, daily, seasonal, and total fluxes of OCS in a forest ecosystem, using a year (2011) of high-frequency, direct measurements at Harvard Forest, MA. We report the seasonal cycle, the response to environmental conditions, and the total deposition flux of OCS throughout the year 2011. We compare these fluxes to corresponding measurements of CO_2 flux and to simulations using the Simple Biosphere model (SiB3).

Results and Discussion

Details of the measurement method and deployment at the Environmental Measurement Site (EMS) flux tower at Harvard Forest are presented in *Methods* and *Supporting Information*.

Seasonal Fluxes of OCS Show Strong Vegetative Uptake. Ecosystem fluxes of OCS (F_{OCS}) varied with air and surface soil temperature through the year and showed complex behavior (Fig. 1). The observed time series of OCS mixing ratios in 2011 followed the typical seasonal cycle measured previously at Harvard Forest (Fig. S1) (1). Total net OCS flux for 2011 was −1.36 ± 0.01 mol OCS per ha per y (−43.5 ± 0.5 g S per ha per y, uptake from the atmosphere). The nighttime flux accounted for −0.38 ± 0.01 mol OCS per ha per y (−12.3 ± 0.4 g S per ha per y), ∼28% of total uptake, peaking in spring and autumn (Fig. 1*B* and *Supporting Information*).

As expected, the largest uptake fluxes were observed during the growing season (Fig. 1), starting in April when conifer trees became active and the snowpack melted to expose the forest soil. Daytime uptake of OCS (Fig. 1*A*) increased through May and June in parallel with photosynthesis, marked by bud break of deciduous trees (May 5) and sharply increased rates of sap flow (May 19). This trend was unexpectedly interrupted by strong emission of OCS during midday hours in late July, when soil moisture was lowest and air temperature was the warmest of the year. As soil moisture gradually increased in August, net OCS uptake resumed in the daytime, but net OCS emission was observed at night (Fig. 1*B*). In September and October, the daily total and daytime OCS uptake flux diminished as air and soil temperature decreased, whereas nighttime OCS uptake resumed. Daytime emissions of OCS were observed yet again in early November, during the senescence of red oak (*Quercus rubra*) leaves, cancelling the nighttime uptake and resulting in a daily mean $F_{OCS} \sim 0$. In mid-December 2011, anomalously low snowfall and above-freezing air and soil temperature appeared to stimulate daytime OCS uptake, possibly reflecting uptake by conifer trees.

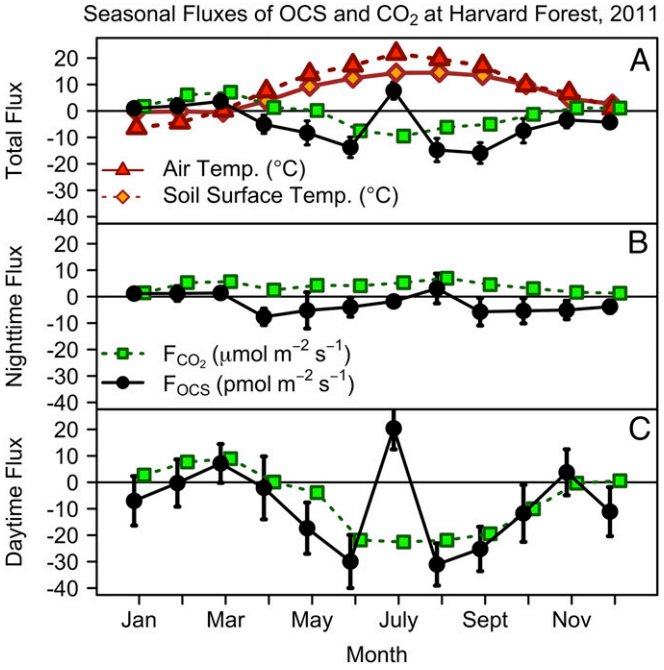

Fig. 1. Monthly mean OCS (F_{OCS}, pmol·m^{-2}·s^{-1}; black) and CO_2 (F_{CO2}, μmol·m^{-2}·s^{-1}; green squares) fluxes for 2011. $u^* > 0.17$ m·s^{-1} for all data. (*A*) Total OCS and CO_2 flux by month. Air temperature (red triangles; °C) and surface soil temperature (orange diamonds; °C); CO_2 net flux includes changes in storage, but this is not required for OCS. (*B*) Nighttime OCS (black) and CO_2 (green) flux (PAR < 40 μE·m^{-2}·s^{-1}). (*C*) Daytime OCS and CO_2 fluxes with PAR > 600 μE·m^{-2}·s^{-1}. Error bars indicate the 95% confidence intervals for all data within the month.

Nighttime OCS Uptake. Nighttime, light-independent uptake of OCS is likely mediated by both soils and vegetation. Nighttime transpiration through incompletely closed stomata has been observed in many tree species (26, 27), and nighttime OCS uptake has been observed in deciduous and conifer forests during the growing season (28). Soil fluxes are significant for both CO_2 and OCS but typically have opposite signs: CO_2 is respired from soils, whereas OCS is generally taken up. Carbonic anhydrase is present in the soil microorganisms typical of oxic soils found at Harvard Forest (29). OCS has been observed to be taken up by oxic soils, but the rate is notably slower on the ecosystem scale than OCS uptake by vegetation (30). Maseyk et al. (8) attributed ∼29% of total OCS flux by winter wheat to nighttime OCS uptake by foliage, with only 1–6% due to soils, at the peak of the growing season (8). The results of these studies generally agree with our results during the growing season. However, the continued strong uptake of OCS from October through December (Table S1), after the decline in activity of the deciduous canopy, implicates soil uptake as a significant portion of annual uptake, when accounting for the dormant season. We infer that uptake by soils, and potentially by conifer leaves, may contribute to the strong vertical gradient in OCS mixing ratios observed over North America from October to December (1).

Separating Vegetative and Soil Uptake of OCS and CO_2. To separate the influence of soil and vegetative processes, we examined time periods when each process dominates: early December (soil uptake dominant), April/November (soil and conifer) and May–October (soil, conifer, and deciduous trees).

In early December, before the air temperature warmed again in mid-December, deciduous leaves were absent, and air temperature was below freezing. The soil temperature at Harvard Forest in 2011 was 2.5 °C higher than the 12-y average (2001–2012) all the way through October and November, encouraging microbial activity late in the year, even when air temperature dropped below freezing. Measurements of sap flow rate (*Supporting Information*) show that the red oak trees activity was sharply diminished after November 13. The early December OCS uptake [7.2 ± 3.4 (95% confidence interval; CI) pmol·m^{-2}·s^{-1}; Fig. S2] was similar to the total ecosystem OCS uptake in late November, with no statistical difference between daytime (6.0 ± 10.9 pmol·m^{-2}·s^{-1}) and nighttime (10.3 ± 7.6 pmol·m^{-2}·s^{-1}) OCS uptake. We infer that the OCS uptake from cold but unfrozen soils is about 7 pmol·m^{-2}·s^{-1}. After the soils froze, the OCS flux was not measurably different from zero throughout the winter (Fig. S2).

In late April, once the soils thawed with warming air temperature and conifer activity began, daytime uptake (18.8 ± 18.0 pmol·m^{-2}·s^{-1}) was greater than nighttime OCS uptake (7.7 ± 5.4 pmol·m^{-2}·s^{-1}), suggesting daytime conifer leaf uptake of 11 ± 18 pmol·m^{-2}·s^{-1}. The late April nighttime uptake, after soils thaw, is comparable to early December total uptake, which we have attributed to soil uptake. However, we were not able to partition the nighttime uptake of OCS into soil and vegetative contributions in late April. This estimate, for active soils in April and December is in close agreement with the average soil uptake measured in a creek area in Colorado (28) of 7 ± 2.6 pmol·m^{-2}·s^{-1} and is slightly greater

than the average uptake rate for soil in a mixed forest reported for China of 4.8 ± 2.9 pmol·m^{-2}·s^{-1} (31).

Dependence of OCS Flux on Wind Direction and Temperature. Fluxes of OCS reveal heterogeneity by wind direction, reflecting the tree species distribution within the flux tower footprint (*Supporting Information*). In June, August, and September, daytime fluxes of OCS for air from the northwest (NW; mixed conifer and deciduous, 40.9 ± 8.2 pmol·m^{-2}·s^{-1}) were almost twice as large as the OCS uptake in air from the southwest (SW; deciduous dominated, 23.5 ± 8.2 pmol·m^{-2}·s^{-1}). By contrast, the net daytime CO_2 flux was roughly the same in both wind directions [F_{CO2} (NW) = −23.0 ± 1.0 μmol·m^{-2}·s^{-1} vs. F_{CO2} (SW) = −22.1 ± 0.9 μmol·m^{-2}·s^{-1}]. The higher daytime OCS uptake flux in air from the NW sector, combined with larger nighttime ecosystem respiration (R_{eco}) from this sector, suggests that the magnitudes of daytime R_{eco} and GEP are both greater in this conifer-dominated sector, compared with the deciduous-dominated SW sector. In this example, F_{OCS} data, combined with F_{CO2} data, provide unique information about the metabolic activity of plant leaves at the ecosystem scale, which are traceable to the controlling factors of photosynthesis. However, careful interpretation is required because F_{OCS} is not a direct measure of photosynthesis.

Fluxes of OCS, CO_2, and GEP showed strong dependence on air temperature (Fig. 2*A*). When the air temperature rose above 16 °C, net F_{CO2} changed from positive (respiration dominated) to negative (photosynthesis dominated). When the canopy was fully developed and leaves in the canopy were most active, uptakes of both OCS and CO_2 were strongest, peaking at the highest temperature, except for the anomalous period in July when OCS was emitted by leaves but CO_2 uptake continued.

Ecosystem OCS Flux Dependence on Light and Stomatal Conductance. Both OCS and CO_2 diffuse from the atmosphere through stomata into leaves, where they are hydrolyzed by the light-independent enzyme carbonic anhydrase (CA). For OCS, the products are H_2S and CO_2, and the process is thought to be irreversible. In contrast, fixation of CO_2 through photosynthesis is a two-step process: diffusion into the leaves, reversible hydration by CA, then light-dependent and irreversible fixation by RuBisCo. Uptake of OCS does not require light, but OCS fluxes covary with light indirectly, via stomatal opening. The OCS flux is largely controlled by the conductance of the stomata in series with the mesophyll (cell walls and membranes), which regulate the rate of diffusion of OCS from the air to the site of the CA reaction. Gas exchange studies with leaves indicate that the mesophyll component of the effective conductance scales with the amount of RuBisCo in leaves of C3 and C4 species. The stomatal component is linked to the instantaneous rate of photosynthesis, humidity, and the chloroplast CO_2 concentration (4).

We infer that measurements of ecosystem OCS fluxes promise to provide new means to determine stomatal conductance on the ecosystem scale. The fluxes of OCS, CO_2, and GEP show strong dependences on photosynthetically active radiation (PAR; Fig. 2*B*), with important differences among them. We observed strong OCS uptake earlier in the day and persisting later in the day than net CO_2 uptake, which is offset by respiration. This behavior was predicted by Goldan et al. (9) and is observed here for the first time to our knowledge at the ecosystem scale (Fig. 2*B*).

We explored the link between F_{OCS} and stomatal conductance using the SiB3 model (Methods). The SiB3 model uses the Ball–Berry equation for stomatal conductance and has a simple parameterization of the mesophyll component. The mean diel cycle of the observed OCS flux and the calculated stomatal conductance are very similar, with enhanced activity at low-light conditions in August and September (Fig. 3*C*). The simulated OCS uptake shows good agreement at times of high light (Fig. 3*A*) but is underestimated compared with the observed fluxes, especially at times of low light and at night (Fig. 3*B*). This highlights the need for model refinements, such as using OCS fluxes to constrain stomatal conductance at night.

Previous laboratory studies had proposed that OCS fluxes should scale directly with stomatal conductance (32, 33); however, this is the first evidence to our knowledge demonstrating this relationship in a forest ecosystem. We find, from the observed nocturnal uptake of OCS by the canopy, strong evidence for, and potential quantification of, incomplete stomatal closure at night. The results support the view that we can use the OCS flux as a means to measure the stomatal conductance independently of the water vapor flux, providing a major advance in our capability to assess ecosystem response to environmental forcing, in a simple model framework.

Normalized Flux of OCS and CO_2. We define the flux per mole in air as $f_X = F_X/[X]$ (units: mol·m^{-2}·s^{-1}), where F_X represents the observed flux of OCS, CO_2, or GEP and $[X]$ is the ambient mole fraction of OCS or CO_2 in dry air. When adjusted for ambient temperature and pressure, this is comparable to the flux per unit molecule (units: m·s^{-1}). For periods when the canopy takes up OCS, the flux per mole represents the apparent canopy conductance of OCS that includes the stomatal, boundary layer, and

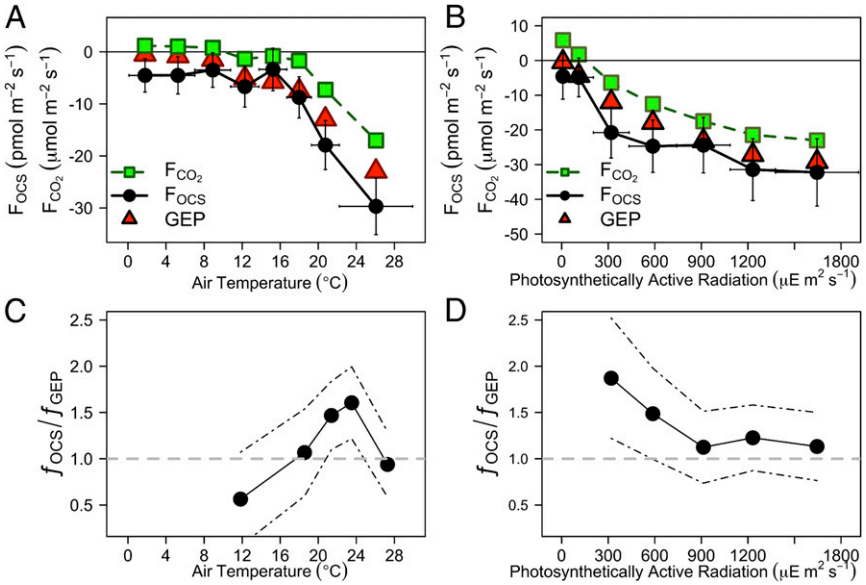

Fig. 2. The relationship of OCS flux (F_{OCS}, pmol·m^{-2}·s^{-1}; black circles), CO_2 flux (F_{CO2}, μmol·m^{-2}·s^{-1}; green squares), and photosynthesis (calculated as GEP, μmol·m^{-2}·s^{-1}; red triangles) with (*A*) air temperature and (*B*) PAR. Values of F_{OCS} and F_{CO2} include nighttime values. (*C*) The f_{OCS}/f_{GEP} ratio with air temperature, for PAR > 300 μE·m^{-2}·s^{-1}. (*D*) The f_{OCS}/f_{GEP} ratio with PAR, for PAR > 300 μE·m^{-2}·s^{-1}. Black dashed lines show 95% CI. July data are excluded. Only data with u^* > 0.17 m·s^{-1} are used.

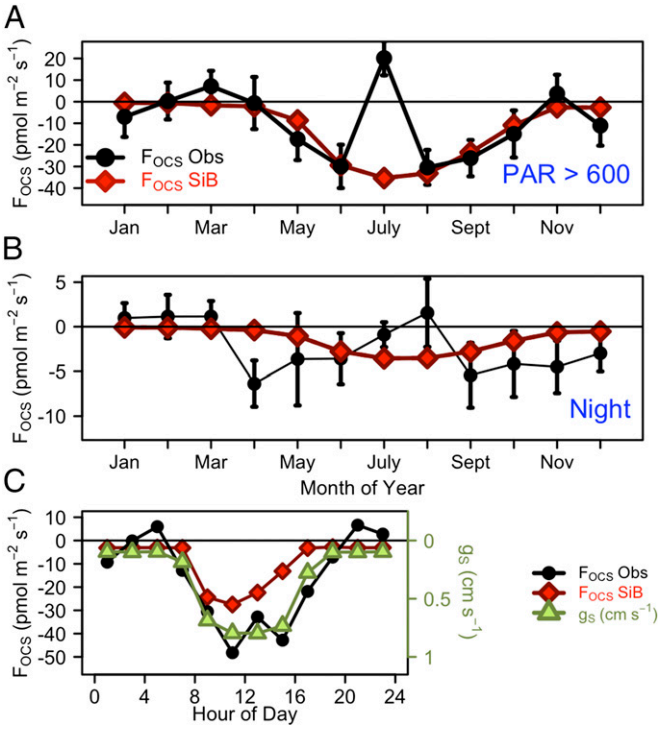

Fig. 3. Monthly mean observed OCS (F_{OCS} Obs, pmol·m^{-2}·s^{-1}; black) and Simple Biosphere (SiB3) model simulated OCS (F_{OCS} SiB, pmol·m^{-2}·s^{-1}; red) fluxes for (*A*) daytime (PAR > 600 μE·m^{-2}·s^{-1}) and (*B*) nighttime. (*C*) Mean diel cycle of observed (black) and simulated (red) OCS fluxes and stomatal conductance of OCS, g_S (cm·s^{-1}; green) for August–September 2011.

internal leaf conductances in series (following equation 3 in ref. 4). We observe that the ratio of the flux per mole of OCS (f_{OCS}) to the gross ecosystem photosynthesis per mole of atmospheric CO_2 (f_{GEP}), the f_{OCS}:f_{GEP} ratio, varied through the season, with relatively high values in May and November (greater relative OCS uptake) decreasing to a (negative) minimum in July (due to OCS emission) (Table S1). The daytime f_{OCS}:f_{GEP} ratio increased with air temperature to 24 °C before decreasing at higher temperatures (Fig. 2*C*), suggesting a physiological optimum. The f_{OCS}:f_{GEP} ratio was not constant with PAR, with the highest values at times of low light, early and late in the day (Fig. 2*D*).

If we assume that changes in soil flux are small across the day compared with the vegetative uptake of OCS, f_{OCS}:f_{GEP} may be compared with the leaf-scale relative uptake (LRU), which can be measured using leaf chambers. Leaf chamber studies reported LRU values of 1–4 over a large range of light conditions and tree species (15) or 1.3–2.3 (28) for a variety of tree species. A field study of wheat reported LRU values of 0.9–1.9 for various light conditions (8). We calculate a mean daytime f_{OCS}:f_{GEP} ratio for air temperatures above 14 °C (i.e., times of full canopy) of 1.4 ± 0.3, within the range of the previous values. The variations in apparent flux ratio are somewhat more complex than commonly assumed, due to the strong light dependence. Nevertheless, they can be well represented in simulations of SiB3 modified to include soil and canopy exchange of OCS (4) (Fig. 3).

Application of OCS Fluxes to Estimation of GEP. Ecosystem-scale fluxes of OCS have been proposed as a means to directly determine the photosynthetic uptake of carbon in the biosphere, independently of soil and plant respiration (1, 13, 14, 19). However, for this approach to work as proposed, a number of requirements must be met, many of which are not realized year-round at Harvard Forest. These conditions include the following: (*i*) F_{OCS} should be unidirectional (i.e., no OCS emission). We observed net OCS emission at times of ecosystem stress. (*ii*) Nighttime uptake of OCS should be negligible or relatively constant and quantifiable. We found nighttime uptake varies throughout the year and accounts for ∼28% of the annual OCS uptake. (*iii*) The LRU of OCS/CO_2 for the ecosystem type should be known. Our study shows that the ecosystem f_{OCS}:f_{GEP}, as related to LRU, is not constant but may be predicted, with observed values falling within the reported range of LRU values, provided that environmental conditions are restricted to air temperature between 14 °C and 28 °C (Fig. 2*B*), PAR > 600 μE·m^{-2}·s^{-1} (Fig. 2*D*), times of full canopy and average soil moisture.

In view of these limitations, we tested the applicability of OCS for the approximation of GEP (GEP_{OCS}) during ideal conditions (high illumination with moderate temperature and soil moisture) in September 2011 (LRU = f_{OCS}:f_{GEP} = 1.5 ± 0.5; Fig. 4). Using the mean LRU of 1.5 calculated for September, the total daily sum of GEP_{OCS} and GEP_{CO2} agrees to within 3.5%, a good agreement given the ∼10% uncertainty estimated for GEP_{CO2} (23). However, this result depends on the value of LRU assumed (8, 19): varying the LRU between 2 and 1 results in a 29% underestimation or a 36% overestimation, respectively (Fig. 4). GEP_{OCS} extends through more of the day than GEP_{CO2} (earlier morning and later evening uptake), highlighting the differing light dependence of uptake pathways of OCS and CO_2 discussed earlier. Thus, the OCS fluxes are closely related to GEP (through stomatal conductance) during the dominant flux-weighted carbon uptake periods, with anomalies to be expected during periods of high stress. The SiB3 model framework evidently offers a way to extend beyond the gross daily averages, as may be desired to understand large-scale ecological processes and their response to environmental and ecological change.

Emission of OCS. Both light-dependent and light-independent mechanisms appear to contribute to the net OCS emissions from the ecosystem observed during an anomalous period in July. Net emissions were observed forest-wide (all wind directions), both day and night, under the conditions of high air temperature (>30 °C) in late July and early August. Net OCS emission was also observed in the deciduous-dominated wind sector in late June and in August and yet again during senescence in November. Heat stress may have been a determining factor in the observed OCS emission in summer, which was strongly enhanced at air temperature above 21 °C. During July 19–31, OCS emission increased with rising vapor pressure deficit (VPD) and bulk sap flow rate for maple trees (Fig. S3). The peak F_{OCS} (+26.3 ± 17.3 pmol·m^{-2}·s^{-1}) coincided with a slight depression in stomatal conductance in the afternoon. In the absence of OCS emission from the ecosystem, the expected daytime net OCS flux due to hydrolysis by CA (based on June and August peak OCS ecosystem uptake) should have been around −30 pmol·m^{-2}·s^{-1}, and hence, the observed net flux of +20 pmol·m^{-2}·s^{-1} in late July could correspond to a maximum gross emission by the responsible mechanisms of 50 pmol·m^{-2}·s^{-1} at midday. A recent study reported OCS emissions from temperature-stressed soils and senescent wheat at harvest time (8, 20). The

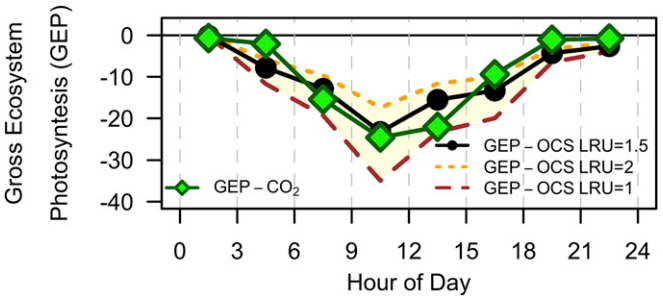

Fig. 4. GEP calculated directly from OCS fluxes (GEP_{OCS}; yellow) with LRU values of 1 (brown long-dashed line), 1.5 (black points), and 2 (orange dashed line) and indirectly extrapolated from nighttime temperature-dependent respiration (GEP_{CO2}; green diamonds) for September 2011.

metabolism of sulfur containing amino acids, which increases with temperature and plant stress, may lead to OCS production (8) in a similar manner to CO (34) and CH_4 production (35) from thermal degradation. However, the emission observed here occurred at temperatures much lower than in the wheat field study. Nighttime OCS emission peaked in August (Fig. 1*B*), when CO_2 respiration was greatest, indicating that there is also a different, light-independent emission mechanism, possibly associated with decomposition.

In early November, OCS emissions of ~5 pmol·m^{-2}·s^{-1} were observed briefly during the leaf senescence of the red oak trees. It is possible this emission occurred through a process similar to that observed during wheat senescence in Oklahoma (8). High surface soil temperature was also implicated as a source of OCS in that study. However, the high soil temperature observed in Oklahoma (45 °C) was never reached at Harvard Forest because the canopy shielded the forest floor from direct light, and there is no correlation of OCS emission with soil temperature in November. Therefore, we suspect that the source of OCS may have been within the senescent canopy or from freshly fallen leaves in the litter layer on the forest floor.

Because the air temperature at Harvard Forest has warmed 1.5 °C over the past 50 years (36, 37) with increasingly large interannual variability, drought and heat stress events may increase in frequency (38). Our results suggest that climate change may shift the balance between OCS uptake and emission processes at Harvard Forest and in similar terrestrial ecosystems, leading to changes in the global OCS budget.

Conclusions

Our year-long measurements at Harvard Forest demonstrate that OCS flux observations provide quantitative, independent measures of metabolic activity and biophysical properties of the forest canopy at the ecosystem scale. We observed net uptake of OCS totaling 1.36 ± 0.01 mol OCS per ha per y (43.5 ± 0.5 g S per ha per y), predominantly in the daytime (72%), with the balance at night attributed to soil consumption and to vegetative uptake through incompletely closed stomata. The flux of OCS was found to be bidirectional, with net emission during very hot, dry conditions and when vegetation senesced in autumn.

Uptake of OCS by a forest canopy is regulated by stomatal conductance, mesophyll conductance, and the activity of carbonic anhydrase, acting in series. At times of peak carbon uptake (full canopy, high illumination, and adequate soil moisture), OCS fluxes are directly proportional to photosynthetic carbon flux, with minor contributions from soils and other processes. However, because OCS uptake does not depend on light levels and Rubisco activity directly as for CO_2, the leaf scale relative uptake (f_{OCS}:f_{GEP}) has systematically higher values at dawn and dusk than at midday and, likewise, spring and fall versus summer.

We found that daytime OCS uptake was well simulated by the Simple Biosphere model (SiB3), using a basic, low-dimensional representation of OCS metabolism by plants. Thus, the observations can quantitatively constrain the aggregated functioning of the photosynthetic apparatus, at ecosystem scale, in the model framework. SiB3 underestimated uptake of OCS at times of low light and at night and did not account for production processes observed under stress conditions and during senescence. Refinement of the model is needed to account for these features, but these influences on total fluxes are relatively modest.

We conclude that OCS fluxes provide a powerful means for quantitatively measuring the large-scale photosynthetic activity of the terrestrial biosphere. By using a proper model formulation, OCS flux measurements over a forest allow us to directly observe and quantify the mechanisms that mediate temporal changes and spatial heterogeneity of canopy gas exchange of CO_2 and H_2O at the ecosystem scale.

Methods

A tunable infra-red laser direct absorption spectrometer (TILDAS; Aerodyne Research Inc.) was used to measure atmospheric mixing ratios and derive gradients and fluxes of carbonyl sulfide and water vapor at 2,048.495 cm^{-1} and 2,048.649 cm^{-1}, respectively. Mixing ratios of OCS and H_2O at a frequency of 4 Hz for eddy covariance flux (eF_{OCS}; August 2011 to December 2011) or 1 Hz for gradient flux (gF_{OCS}; January 2011 to August 2011) were calculated using TDL Wintel software (Aerodyne Research Inc.). The 1σ instrument precision was typically 14 ppt at 4 Hz, averaging down to <1 ppt at 60 s. The sensor is a further development of earlier instruments (17, 18). More details about the measurement technique and associated instrumental tests and the theory behind the flux calculations are provided in *Supporting Information* and Figs. S4–S7. Tests were conducted to ensure continuity of measurement techniques. A comparison of the OCS mixing ratios (TILDAS) observed at the same time as National Oceanic and Atmospheric Administration (NOAA) flask samples is shown in Fig. S1.

Measurements were made at the Environmental Measurement Site (EMS) at Harvard Forest, Petersham, MA (42.54°N, 72.17°W, elevation 340 m). The CO_2 flux has been measured at this Long-Term Ecological Research (LTER) site since 1990 (24). Details about the site, environmental conditions, and ancillary measurements during the study period are described in *Supporting Information*. Environmental conditions for the study were typical of New England. Up to 75 cm of snow accumulated between January and April in 2011. The air temperature ranged from −28 °C in January to 35 °C in July. At Harvard Forest, conifer trees are generally not active when the air temperature is consistently below 0 °C (39). The CO_2 flux from soil respiration depends mainly on microbial activity and CO_2 diffused through the snowpack, with increased exchange from wind pumping. Microbial activity continued through the winter as the soil temperature was partially shielded from the low air temperature by the insulating snow pack (40) before the frost depth extended down to 10 cm into the soil in early March. Bud break was observed for deciduous species around May 5, and senescence began late in October. Prolonged power loss resulted from damage to power lines and damage to electronic equipment due to lightning on May 28. Because no OCS fluxes were measured during the first 2 wk of May and again the first 2 wk of June, the mean uptake for both May and June was based only on measurements during the last half of each month.

There was less than 60 mm precipitation during June and July, and this precipitation was concentrated into four short events. Prolonged high temperature (>30 °C) affected the site in mid-July, resulting in low soil moisture in the area. Storms arrived in early August, bringing prolonged and heavy precipitation and increasing soil moisture. Hurricane Irene on August 28 caused extensive flooding in the region. October was unseasonably warm, and leaves were still on trees when a snowstorm on October 29 brought almost 50 cm of snow to the area, again resulting in a brief power cut at the site and flooding in the area on thaw. Although soils were dry in July, these large moisture events resulted in greater cumulative precipitation for 2011 (1,635 mm) than the 10-y average for the site (1,226 mm).

OCS fluxes derived during times of low turbulence ($u^* < 0.17$ m·s^{-1}) and during periods of precipitation were removed (21), leaving valid data covering 34% of the 30-min periods over the entire year, slightly less than the 45% reported by Urbanski et al. (24) as the mean valid CO_2 flux data points for the years 1992–2004. The valid data (approximately six thousand 30-min values) were uniformly distributed over the year, and every hour for each composite month throughout the year had valid OCS flux data, allowing the yearly flux of OCS to be calculated for 2011 as −136 μmol·m^{-2}·y^{-1}, corresponding to a net uptake of 43.5 ± 0.5 g S (as OCS) per ha per y or 16.3 ± 0.1 g C (as OCS) per ha per y by the biosphere. The total CO_2 uptake for the year, selected from times of valid OCS fluxes, was 22.6 mol·m^{-2}·y^{-1} or 2.7 Mg C per ha per y for 2011. This value is within the observed range of net CO_2 uptake of 1.0–4.7 Mg C per ha per y for the years 1992–2004 (25). Overall, the OCS fluxes had a greater relative uncertainty than fluxes of CO_2, reflecting a combination of both a less precise measurement of the OCS flux (the gradient flux calculated OCS flux has more uncertainty than the eddy covariance calculated OCS flux) and more variability of the actual daytime OCS fluxes.

The Simple Biosphere Model version 3 (SiB3), adapted to include OCS, was run using 2011 meteorology data from Harvard Forest (41). SiB3 links stomatal conductance (both C3 and C4) to the energy budget (42, 43) and incorporates satellite-specified phenology (44). Stomatal conductance, determined by the Ball–Berry equation (45), has a direct dependence on relative humidity and CO_2 concentration and indirect dependence on soil water, temperature, light, and humidity through the assimilation term. Both leaf and soil uptake of OCS are explicitly represented in SiB3 (4) independently with the same mechanistic framework as CO_2 but with differing mass, geometry, and reactivity (OCS only reacts with CA). The OCS soil flux represents soil uptake only, and there is as yet no mechanism to represent emission of OCS from soils or the whole ecosystem (e.g., the net emission in July is not captured).

ACKNOWLEDGMENTS. We thank Mark Vanscoy for help with the long-term operation of the instrument at Harvard Forest and flask sampling, Carolina Siso for analysis at National Oceanic and Atmospheric Administration (NOAA), Brad Hall for OCS standardization at NOAA, Ryan McGovern at

Aerodyne for instrumental repairs, and Richard Wehr for helpful discussion. The instrument was developed and deployed as part of US Department of Energy (DOE) Small Business Innovation Research DE-SC0001801. Funding for flask analysis was provided in part by NOAA Climate Program Office's Atmospheric Chemistry, Carbon Cycle and Climate (AC4) Program. EMS tower and CO_2 flux measurements are a component of the Harvard Forest Long-Term Ecological Research site supported by the National Science Foundation (NSF) and additionally by the Office of Science (Biological and Environmental Research), DOE. P.H.T. was supported by a Charles Bullard fellowship at Harvard University during the writing of this manuscript. I.T.B. was sponsored by the NSF Science and Technology Center for Multi-scale Modeling of Atmospheric Processes, managed by Colorado State University under Cooperative Agreement ATM-0425247.

1. Montzka SA, et al. (2007) On the global distribution, seasonality, and budget of atmospheric carbonyl sulfide (COS) and some similarities to CO_2. *J Geophys Res* 112(D9): D09302.
2. Barkley MP, Palmer PI, Boone CD, Bernath PF, Suntharalingam P (2008) Global distributions of carbonyl sulfide in the upper troposphere and stratosphere. *Geophys Res Lett* 35(14):L14810.
3. Brühl C, Lelieveld J, Crutzen PJ, Tost H (2012) The role of carbonyl sulphide as a source of stratospheric sulphate aerosol and its impact on climate. *Atmos Chem Phys* 12(3): 1239–1253.
4. Berry J, et al. (2013) A coupled model of the global cycles of carbonyl sulfide and CO_2: A possible new window on the carbon cycle. *J Geophys Res Biogeosci* 118(2):842–852.
5. Li X, Liu J, Yang J (2006) Variation of H2S and COS emission fluxes from Calamagrostis angustifolia Wetlands in Sanjiang Plain, Northeast China. *Atmos Environ* 40(33): 6303–6312.
6. Whelan ME, Min D-H, Rhew RC (2013) Salt marsh vegetation as a carbonyl sulfide (COS) source to the atmosphere. *Atmos Environ* 73(C):131–137.
7. Liu J, et al. (2010) Exchange of carbonyl sulfide(COS) between the atmosphere and various soils in China. *Biogeosciences* 7(2):753–762.
8. Maseyk K, et al. (2014) Sources and sinks of carbonyl sulfide in an agricultural field in the Southern Great Plains. *Proc Natl Acad Sci USA* 111(25):9064–9069.
9. Goldan PD, Fall R, Kuster WC, Fehsenfeld FC (1988) Uptake of COS by growing vegetation: A major tropospheric sink. *J Geophys Res* 93(D11):14186–14192.
10. Kettle AJ, Kuhn U, von Hobe M, Kesselmeier J, Andreae MO (2002) Global budget of atmospheric carbonyl sulfide: Temporal and spatial variations of the dominant sources and sinks. *J Geophys Res* 107(D22):4658.
11. Kuhn U, et al. (1999) Carbonyl sulfide exchange on an ecosystem scale: Soil represents a dominant sink for atmospheric COS. *Atmos Environ* 33(6):995–1008.
12. Protoschill-Krebs G, Wilhelm C, Kesselmeier J (1996) Consumption of carbonyl sulphide (COS) by higher plant carbonic anhydrase (CA). *Atmos Environ* 30(18):3151–3156.
13. Campbell JE, et al. (2008) Photosynthetic control of atmospheric carbonyl sulfide during the growing season. *Science* 322(5904):1085–1088.
14. Sandoval-Soto L, et al. (2005) Global uptake of carbonyl sulfide (COS) by terrestrial vegetation: Estimates corrected by deposition velocities normalized to the uptake of carbon dioxide (CO_2). *Biogeosciences* 2(2):125–132.
15. Stimler K, Montzka SA, Berry JA, Rudich Y, Yakir D (2010) Relationships between carbonyl sulfide (COS) and CO_2 during leaf gas exchange. *New Phytol* 186(4):869–878.
16. Blonquist JM, Jr, et al. (2011) The potential of carbonyl sulfide as a proxy for gross primary production at flux tower sites. *J Geophys Res* 116(G4):G04019.
17. Stimler K, Nelson DD, Yakir D (2009) High precision measurements of atmospheric concentrations and plant exchange rates of carbonyl sulfide using mid-IR quantum cascade laser. *Glob Change Biol* 16(9):2496–2503.
18. Commane R, et al. (2013) Carbonyl sulfide in the planetary boundary layer: Coastal and continental influences. *J Geophys Res Atmos* 118(14):8001–8009.
19. Asaf D, et al. (2013) Ecosystem photosynthesis inferred from measurements of carbonyl sulphide flux. *Nat Geosci* 6(3):186–190.
20. Billesbach DP, et al. (2014) Growing season eddy covariance measurements of carbonyl sulfide and CO_2 fluxes: COS and CO_2 relationships in Southern Great Plains winter wheat. *Agric For Meteorol* 184:48–55.
21. Goulden ML, Munger JW, Fan S-M, Daube BC, Wofsy SC (1996) Measurements of carbon sequestration by long-term eddy covariance: Methods and a critical evaluation of accuracy. *Glob Change Biol* 2(3):169–182.
22. Reichstein M, et al. (2005) On the separation of net ecosystem exchange into assimilation and ecosystem respiration: Review and improved algorithm. *Glob Change Biol* 11(9):1424–1439.
23. Desai AR, et al. (2008) Cross-site evaluation of eddy covariance GPP and RE decomposition techniques. *Agric For Meteorol* 148(6-7):821–838.
24. Urbanski S, et al. (2007) Factors controlling CO_2 exchange on timescales from hourly to decadal at Harvard Forest. *J Geophys Res* 112(G2):G02020.
25. Keenan TF, et al. (2013) Increase in forest water-use efficiency as atmospheric carbon dioxide concentrations rise. *Nature* 499(7458):324–327.
26. Caird MA, Richards JH, Donovan LA (2007) Nighttime stomatal conductance and transpiration in C3 and C4 plants. *Plant Physiol* 143(1):4–10.
27. Daley MJ, Phillips NG (2006) Interspecific variation in nighttime transpiration and stomatal conductance in a mixed New England deciduous forest. *Tree Physiol* 26(4): 411–419.
28. Berkelhammer M, et al. (2014) Constraining surface carbon fluxes using in situ measurements of carbonyl sulfide and carbon dioxide. *Global Biogeochem Cycles* 28(2):161–179.
29. Smith KS, Jakubzick C, Whittam TS, Ferry JG (1999) Carbonic anhydrase is an ancient enzyme widespread in prokaryotes. *Proc Natl Acad Sci USA* 96(26):15184–15189.
30. Van Diest H, Kesselmeier J (2008) Soil atmosphere exchange of carbonyl sulfide (COS) regulated by diffusivity depending on water-filled pore space. *Biogeosciences* 5(2): 475–483.
31. Yi Z, et al. (2007) Soil uptake of carbonyl sulfide in subtropical forests with different successional stages in south China. *J Geophys Res* 112(D8):D08302.
32. Seibt U, Kesselmeier J, Sandoval-Soto L, Kuhn U, Berry JA (2010) A kinetic analysis of leaf uptake of COS and its relation to transpiration, photosynthesis and carbon isotope fractionation. *Biogeosciences* 7(1):333–341.
33. Stimler K, Berry JA, Yakir D (2012) Effects of carbonyl sulfide and carbonic anhydrase on stomatal conductance. *Plant Physiol* 158(1):524–530.
34. Conrad R, Seiler W (1985) Characteristics of abiological carbon monoxide formation from soil organic matter, humic acids, and phenolic compounds. *Environ Sci Technol* 19(12):1165–1169.
35. Nisbet RER, et al. (2009) Emission of methane from plants. *Proc Biol Sci* 276(1660): 1347–1354.
36. Boose E, Gould E (1999), Shaler Meteorological Station at Harvard Forest 1964-2002 (Harvard Forest, Petersham, MA), Harvard Forest Data Archive HF000. Available at harvardforest.fas.harvard.edu:8080/exist/apps/datasets/showData.html?id=hf000.
37. Boose E (2001), Fisher Meteorological Station at Harvard Forest since 2001 (Harvard Forest, Petersham, MA), Harvard Forest Data Archive HF001. Available at harvardforest.fas.harvard.edu:8080/exist/apps/datasets/showData.html?id=hf001.
38. Diffenbaugh SN, Scherer M (2013) Likelihood of July 2012 U.S. temperatures in preindustrial and current forcing regimes. *Bull Am Meteorol Soc* 94(9):S6–S9.
39. Hadley JL (2000) Effect of daily minimum temperature on photosynthesis in eastern hemlock (*Tsuga canadensis* L.) in autumn and winter. *Arct Antarct Alp Res* 32(4): 368–374.
40. Sharratt BS, Baker DG, Wall DB, Skaggs RH, Ruschy DL (1992) Snow depth required for near steady-state soil temperatures. *Agric For Meteorol* 57(4):243–251.
41. Farquhar GD, von Caemmerer S, Berry JA (1980) A biochemical model of photosynthetic CO2 assimilation in leaves of C 3 species. *Planta* 149(1):78–90.
42. Collatz GJ, Ribas-Carbo M, Berry JA (1992) Coupled photosynthesis-stomatal conductance model for leaves of C4 plants. *Aust J Plant Physiol* 19(5):519–538.
43. Collatz GJ, Ball JT, Grivet C, Berry JA (1991) Physiological and environmental regulation of stomatal conductance, photosynthesis and transpiration: A model that includes a laminar boundary layer. *Agric For Meteorol* 54(2-4):107–136.
44. Sellers PJ, et al. (1996) A revised land surface parameterization (SiB2) for atmospheric GCMS. Part I: Model formulation. *J Clim* 9(4):676–705.
45. Ball JT, Woodrow IE, Berry JA (1987) A model predicting stomatal conductance and its contribution to the control of photosynthesis under different environmental conditions. *Progress in Photosynthesis Research* (Springer, Dordrecht, The Netherlands), pp 221–224.
46. Meyers TP, Hall ME, Lindberg SE, Kim K (1996) Use of the modified Bowen-ratio technique to measure fluxes of trace gases. *Atmos Environ* 30(19):3321–3329.
47. Meredith LK, et al. (2014) Ecosystem fluxes of hydrogen: A comparison of flux-gradient methods. *Atmos Meas Tech* 7(9):2787–2805.
48. Goldstein AH, Daube BC, Munger JW, Wofsy SC (1995) Automated in-situ monitoring of atmospheric non-methane hydrocarbon concentrations and gradients. *J Atmos Chem* 21(1):43–59.
49. Goldstein AH, Fan S-M, Goulden ML (1996) Emissions of ethene, propene, and 1-butene by a midlatitude forest. *J Geophys Res* 101(D10):9149–9157.
50. Goldstein AH, Goulden ML, Munger JW, Wofsy SC, Geron C (1998) Seasonal course of isoprene emissions from a midlatitude deciduous forest. J Geohphys Res 103(D23): 31045–31056.
51. McKinney KA, Lee BH, Vasta A, Pho TV, Munger JW (2011) Emissions of isoprenoids and oxygenated biogenic volatile organic compounds from a New England mixed forest. *Atmos Chem Phys* 11(10):4807–4831.
52. Wilczak J, Oncley S, Stage S (2001) Sonic Anemometer Tilt Correction Algorithm. *Boundary Layer Meteorol* 99(1):127–150.
53. Belviso S, Nguyen BC, Allard P (1986) Estimate of carbonyl sulfide (OCS) volcanic source strength deduced from OCS/CO2 ratios in volcanic gases. *Geophys Res Lett* 13(2):133–136.
54. Contosta AR, Frey SD, Ollinger SV, Cooper AB (2012) Soil respiration does not acclimatize to warmer temperatures when modeled over seasonal timescales. *Biogeochemistry* 112(1-3):555–570.
55. Mellillo JM, Steudler PA (1989) The effect of nitrogen fertilization on the COS and CS2 emissions from temperature forest soils. *J Atmos Chem* 9(4):411–417.
56. Sakai RK, Fitzjarrald DR, Moore KE (2001) Importance of low-frequency contributions to eddy fluxes observed over rough surfaces. *J Appl Meteorol* 40(12):2178–2192.
57. Fierer N, Jackson RB (2006) The diversity and biogeography of soil bacterial communities. *Proc Natl Acad Sci USA* 103(3):626–631.
58. Hutyra LR, et al. (2008) Resolving systematic errors in estimates of net ecosystem exchange of CO2 and ecosystem respiration in a tropical forest biome. *Agric For Meteorol* 148(8-9):1266–1279.
59. Tang J, et al. (2006) Sap flux–upscaled canopy transpiration, stomatal conductance, and water use efficiency in an old growth forest in the Great Lakes region of the United States. *J Geophys Res* 111(G2):G02009.
60. Granier A (1987) Evaluation of transpiration in a Douglas-fir stand by means of sap flow measurements. *Tree Physiol* 3(4):309–320.

Supporting Information

Commane et al. 10.1073/pnas.1504131112

Technical Details

Instrument Description. A TILDAS (Aerodyne Research Inc.) was used to measure atmospheric mixing ratios and derive gradients and fluxes of carbonyl sulfide and water vapor at 2,048.495 cm^{-1} and 2,048.649 cm^{-1}, respectively. There were no CO_2 absorption lines in the spectral range of this laser. Mixing ratios of OCS and H_2O at a frequency of 4 Hz (eddy flux) or 1 Hz (gradient flux) were calculated using TDL Wintel software (Aerodyne Research Inc.). A background spectrum (30-s duration) was obtained every 10 min and interpolated and subtracted from the sample spectra to account for any temporal changes in instrument response. A diaphragm pump was used for gradient flux measurements, which resulted in a flow rate of ∼3 standard liters per minute (slm) and cell response time of 15 s (90% response time). The first 60 s at each level were discarded to allow for equilibration of water vapor. The 1σ instrumental precision was 5 pptv ($pmol{\cdot}mol^{-1}$) in 1-s averaging down to 0.9 pptv at 100 s. During eddy flux measurements, a TriScroll 600-slm pump resulted in a flow rate of 12 slm through the cell and a response time of 1 s. The 1σ instrument precision was typically 14 pptv at 4 Hz, likewise averaging down to <1 pptv at 60 s. The sensor is a further development of previous work (17, 18).

The combined water vapor dilution and pressure broadening correction factor was 1.27 at this wavelength, which, if not corrected, could have caused an underestimation of 7 pptv (in 400 pptv) OCS for 14 ppth ($mmol{\cdot}mol^{-1}$) water vapor. This correction has been applied to the dataset. A NOAA-calibrated cylinder of OCS in air was regularly added to the gradient flux setup (flow rate ∼3 slm); however, the high flow rate of the eddy flux method (∼12 slm from August 4) made frequent overblowing of the inlet with a constant flow difficult and expensive. Instead, the regular additions of OCS-free air for the null spectra were used to determine the temporal variations in the instrument stability, with less frequent addition of the calibration gas. These calibrations were independent of the NOAA flask samples described below.

Fig. S1 shows a time series of OCS measured by the TILDAS (30-min average) and OCS measured in weekly/fortnightly paired flask samples analyzed by gas chromatography with mass spectrometric detection at NOAA [update of measurements from Montzka et al. (1)]. Most flask samples were collected at midday over a few minutes, after extensive flushing. The TILDAS measurements show short-term variability, often greatest outside of midday, that cannot be observed by the flasks. However, when the TILDAS data are averaged for the time periods around the flask sampling time (gray circles in Fig. S1), both measurements track well.

Calculation of OCS Fluxes. Two methods were used to calculate the canopy scale flux of OCS (F_{OCS}) at Harvard Forest. The gradient flux method was used between January 2011 and early August 2011, followed by the eddy covariance method, which continued until the end of the year.

Gradient flux method. The micrometeorological gradient flux method, also known as the modified Bowen ratio method (46), is based on the assumption of trace gas similarity between OCS and, in our measurements, H_2O to calculate the flux of OCS, gF_{OCS} ($pmol{\cdot}m^{-2}{\cdot}s^{-1}$):

$$gF_{OCS} = F_{H_2O}\ gOCS/gH_2O, \qquad \textbf{[S1]}$$

where gOCS ($pmol{\cdot}mol^{-1}{\cdot}m^{-1}$) and gH_2O ($mmol{\cdot}mol^{-1}{\cdot}m^{-1}$) are the vertical concentration gradients of OCS and H_2O, respectively, measured simultaneously by the TILDAS at two heights (29.5 m and 24.1 m),

$$gX = [X]_{29.5m} - [X]_{24.1m}/(29.5 - 24.1), \qquad \textbf{[S2]}$$

and the water vapor flux F_{H2O} is measured directly by eddy covariance at the EMS tower using a infrared gas analyzer [IRGA; Li-COR 6262 (24)]. The nominal TILDAS water vapor mixing ratios were 22% higher than the calibrated water vapor mixing ratios measured by the IRGA. The water vapor observed by the TILDAS was based on spectroscopic parameters and was not externally calibrated, so this correction was applied to the TILDAS water vapor mixing ratios before calculation of the gradient flux.

The OCS flux could not be calculated for 23% of the OCS measurements made during the May–August 2011 sampling period. This was due to a combination of rain events (when no water vapor flux was calculated) and unrealistic water vapor mixing ratios (ΔH_2O outside the 95% quantiles of the total data), which resulted in equally unrealistic OCS fluxes. Fig. S4 shows the diel cycle of the measurements of OCS gradient (Fig. S4*A*) and H_2O gradient (Fig. S4*B*), the H_2O flux measured by eddy flux (Fig. S4*C*), and the calculated OCS flux using the gradient flux method (Fig. S4*D*) for June 14, 2011. The CO_2 flux measured by eddy covariance (Fig. S4*E*) is included for comparison. Negative fluxes indicate loss from the atmosphere and uptake by the biosphere.

The overall uncertainty of the gradient flux method was calculated for each point as the root-mean-square of the 95% confidence intervals of the gradient measurements (gOCS and gH_2O) and the mean error of the eddy covariance calculated water vapor [15% (24)]. As the instrument is optimized to OCS detection, the error in the water vapor gradient measurement, combined with the SD of the water vapor mixing ratio within a 30-min period, dominated the overall uncertainty. For the June–July period, the uncertainty in absolute fluxes ranged from 0.05 $pmol{\cdot}m^{-2}{\cdot}s^{-1}$ to 20 $pmol{\cdot}m^{-2}{\cdot}s^{-1}$ on rare occasions with a median of 0.43 $pmol{\cdot}m^{-2}{\cdot}s^{-1}$. For example, as shown in Fig. S4, this uncertainty reaches a maximum of 5.7 $pmol{\cdot}m^{-2}{\cdot}s^{-1}$ for an OCS flux of 1.1 $pmol{\cdot}m^{-2}{\cdot}s^{-1}$ on June 14, 2011.

For the gradient flux method, ambient air was alternatively sampled from the tower heights of 29.5 m and 24.1 m using 40 m of 3/8" (OD; 0.95 cm) Synflex tubing. Teflon particle filters (pore size 5 μm) at the inlet of each sampling line were changed every 2–4 wk to prevent artificial production of OCS on chemically aged or dirty surfaces (*Artificial OCS Production*). These filters resulted in a pressure drop through the tubing, which reduced the effects of adsorption/desorption on the tubing. The black Synflex tubing also reduced any sunlight effects on the sample. The air in each sampling tube was tested after each background (10- or 30-min interval) to ensure no in situ production of OCS (short-lived increase in OCS). The materials in the instrument were carefully chosen to minimize any artifacts during sampling: clean Teflon filters, Synflex tubing, stainless steel solenoid valves, and the glass sampling cell were not found to scavenge or emit OCS. No pump was used upstream of sampling to prevent contamination of the sample gas. Some initial measurements were made at 25 m and 1 m during the winter of 2010–2011. The calculated fluxes for this winter 2011 period agreed with eddy fluxes for winter 2012, so these early data have been included in the seasonal cycle of F_{OCS}. For eddy covariance flux measurements, only the 29.5-m inlet was used.

The gradient flux method has been used successfully at Harvard Forest previously to measure fluxes of hydrogen (47), nonmethane hydrocarbons (48, 49), and isoprene (50). In each of these studies, the use of CO_2, H_2O, and air temperature produced similar fluxes throughout the year with varying precision and accuracy. These methods were further validated by McKinney et al. (51), who found very similar fluxes of isoprene using a disjunct eddy covariance method, compared with Goldstein's gradient flux method. Particularly relevant to the study here, Meredith et al. (47) found that the gradient flux method using either H_2O or CO_2 was valid throughout 2011.

To test scalar similarity using water vapor during the anomalous hot period in July, we calculated the OCS flux using the CO_2 gradient and flux from the eddy covariance system (Fig. S5). The CO_2 gradients are smaller than H_2O, and the top levels are measured less frequently, which introduces additional noise to the calculated flux compared with the flux calculated from H_2O. The OCS flux calculated based on CO_2 shows the same seasonal cycle for both day and night data as OCS from water vapor but with substantially more noise in the CO_2-based flux, as expected. Fig. S5 shows F_{OCS} for the July 21–31 OCS emission period calculated from H_2O ($FOCS_{H2O}$) and CO_2 ($FOCS_{CO2}$). Regardless of the method used, statistically significant emission of OCS was observed throughout the day in the July period.

Eddy covariance method. The eddy covariance fluxes of OCS (eF_{OCS}) and H_2O (eF_{H2O}) were calculated from high-frequency (4 Hz) measurements of OCS and H_2O made by the TILDAS at 29.5 m. After subtracting a block average for the interval, the covariance of the residual of the vertical wind velocity (w′) and concentration (OCS′ or H_2O') for each 30-min interval was calculated as in Goulden et al. (21), e.g.,

$$F_{OCS} = \overline{w'OCS'} \quad eF_{OCS} = w'\mathrm{OCS} \quad eF_{H_2O} = w'H_2O'. \qquad \textbf{[S3]}$$

The instrument synchronization time lag was determined by maximizing the correlation between w′ and H_2O'. This lag also accounted for differences in computer clock times between the sonic and OCS data systems, which increased gradually after each synchronization reset (daily). The flux is rotated to the plane where the mean vertical wind is zero (52). The calibrated IRGA water vapor fluxes were used for all analysis. Accurate fluxes can be calculated even though high-frequency noise limits the precision of the OCS concentration at short times because the noise is not correlated with vertical wind velocity. The error in the eddy covariance was determined by calculating the root-mean-square combination of observed covariance for periods ±25 s from the lag time. This resulted in a mean SE in the eddy covariance calculated OCS flux of 14%.

Gradient flux and eddy covariance comparison. Both gradient measurements and eddy flux measurements were made for a limited time period, 6–12 August 2011, when additional measurements were made at a height of 24.1 m for 120 s every 30 min. This shorter sampling period at 24.1 m resulted in a greater error in the gradient flux (gF_{OCS}) for this period (47). In a comparison of the two methods, the composite diel cycle (2 hourly bins) of gF_{OCS} (Fig. S6, black circles) and eF_{OCS} (Fig. S6, red boxes) for periods of common measurements showed similar behavior but with slightly more variance in gF_{OCS}, as expected. The overall trend through the composite day compares well for both methods, with no statistical difference between the daily mean flux calculated by either method: daily mean OCS uptake of −8.6 (± 6.2; 95% CI) pmol·m^{-2}·s^{-1} for gF_{OCS} and −9.6 (± 4.4) pmol·m^{-2}·s^{-1} for eF_{OCS}. The gradient flux of OCS underestimates the total daily flux (gF_{OCS} = −174 pmol·m^{-2}·s^{-1}) by 7% compared with the eddy flux (eF_{OCS} = −187 pmol·m^{-2}·s^{-1}). The signs and the diel patterns of the flux are consistent for both methods, except during transition periods near sunrise and sunset when fluxes, especially the water vapor flux used to calculate gF_{OCS}, are small and neither method is reliable.

OCS storage. The actual net uptake or emission of a trace gas by the ecosystem is the observed vertical flux plus any accumulation (or depletion) in the canopy space below the flux sensor (storage term). For CO_2, the storage term is significant compared with the vertical flux, especially around dawn and dusk transitions, disregarding nonideal conditions with significant horizontal advective fluxes. Although the storage term sums to nearly 0 over a daily interval, it must be included to interpret net CO_2 exchange on subdaily intervals. During summer 2012 (and when large CO_2 storage values were calculated), changes in storage of OCS calculated from OCS profile measurements were negligible. The physical processes affecting storage should not change from year to year, so the contribution to the ecosystem flux of OCS from 2012 should be applicable to 2011. Therefore, storage has been neglected in the OCS flux results that we report here.

Artificial OCS Production. Heterogeneous production of OCS on the surface of the contaminated Teflon filters was observed over 5 d after sampling an anthropogenically influenced air mass in February 2011 because unsafe climbing conditions prevented immediate replacement of the filter, which had been in place since late December. This OCS production was observed as large, short-lived pulses of OCS (up to 800 pptv) when sampling the line (and contaminated filter) after zero air background measurements. However, no evidence of OCS production from filter contamination was observed during the summer emission period described in the main text. Air mass trajectories for this February event indicate that the air was influenced by high sulfur emission from the copper and nickel smelters in Sudbury, ON, Canada, and SO_2 mixing ratios of greater than 60 ppbv were observed in the same air mass at a site 60 miles east of Harvard Forest (Aerodyne Research) on the same day. OCS dissolves, but is not hydrolyzed, in acidic water. Belviso et al. (53) measured supersaturated OCS in acidic rainwaters in France and suggested an in situ production of OCS from the acid catalyzed reaction of thiocyanate salts. No further studies have confirmed this suggested mechanism. However, the emission of high mixing ratios of OCS from Teflon filters could be related to a similar production mechanism because OCS production continued for a number of days and was increased in warmer, and slightly more humid, daylight conditions. There is limited literature on the heterogeneous production of OCS and potential mechanisms should be investigated in future studies. Data with contaminated filter production of OCS have been removed from further analysis and from Fig. S1.

Materials for the instrumental setup were carefully chosen to ensure no artificial production of OCS in the system. Testing showed that OCS was produced by rubber diaphragms in pumps and resulted in strong OCS production (pulses up to 24 ppb) in recirculating soil chambers at Harvard Forest. No soil chamber data were used in the analysis presented here. Neoprene and plastic tubing, which are often used in soil chambers, were particularly strong producers of OCS. Clean Synflex and Teflon tubing were not found to produce observable OCS. Although steps have been taken to minimize the effect of material contamination and to remove any data influences by atmospheric contamination, it is possible that the large OCS emission observed in July may be the result of some unknown physical production mechanism. In their studies of OCS in a wheat field, Maseyk et al. (8) observed OCS emission of 217 μg S per m^2 over the final 10 d of measurements (from a total of 657 μg S per m^2 over 7 wk). We estimate a comparable OCS emission of 207 μg S per m^2 over the 10 d of observed net OCS emission at Harvard Forest.

Soil warming and nitrogen fertilization experiments have been conducted in plots to the SW of the tower from 2006 to present, including during 2011 (54). These experiments use ammonium nitrate (NH_4NO_3) to fertilize 12 plots of size 3 × 3 m. The fertilizer

contains trace levels of sulfur (~0.002% sulfur as SO_4^-), which is equivalent to an application of 2.2 g S per ha per y, a less than 0.01% increase on the sulfur content of the soil. The periods of OCS emissions were not found to correlate with the application of the fertilizer. Although we cannot discount the possibility of an OCS artifact from the fertilizer, we suspect that the small area involved and the low levels of sulfur application are too small to contribute to the observed OCS signal. Nitrogen fertilization experiments also found increased OCS emission from soils (55), but we do not see a correlation with soil temperature and the related increase in microbial activity. It is possible that the sulfur present in the soils at Harvard Forest, like the soils of the wheat fields in Oklahoma (8), is a source of OCS through some unknown biophysical mechanism.

Site Description and Ancillary Measurements

Site Description. Measurements were made at the Environmental Measurement Site (EMS) at Harvard Forest, Petersham, MA (42.54°N, 72.17°W, elevation 340 m). The CO_2 flux into and out of the forest has been measured at this LTER site since 1990 (24). The 30-m meteorology tower extends about 5 m over the forest canopy and is located on moderately hilly terrain surrounded by several kilometers of relatively undisturbed forest; ~80% of the turbulent fluxes are produced within 0.7–1 km of the tower (56). The basal area ($m^2 \cdot ha^{-1}$) of various tree species within the footprint of the tower is tracked on plots established in 1993. In 2011, the southwest sector was dominated by deciduous species red oak (20.0% basal area) and red maple (11.8%) with some black oak (2.6%) and ash (2.1%). The northwest sector was more mixed with red oak (17.3%) and hemlock (13.2%) dominating and some red maple (9%), red pine (7.3%), and white pine (5.4%). A dried up pond, which is now an area of new tree growth, was also located in the northwest sector.

Soils at Harvard Forest are acidic and originate from sandy loam glacial till. The diversity and richness of the soil microbial community is somewhat reduced at low soil pH (57), but the soil at Harvard Forest contains representatives of the phyla typical in most soils, many of which can encode for one or more carbonic anhydrase enzymes (29).

CO_2 Flux Measurements. The CO_2 flux at the EMS tower was measured by eddy covariance as described extensively in previous work (21, 24) and in Figs. S5–S7. The CO_2 flux term accounts for storage of CO_2 within the canopy as determined from gradient measurements of the CO_2 concentration (58). The daytime respiration of CO_2 is projected from the observed temperature dependence of respiration at night. To estimate gross ecosystem productivity (GEP) from the measured CO_2 flux, we use the difference between the daytime CO_2 flux and the projected daytime respiration (21).

The Hemlock Tower is another flux tower at Harvard Forest located 500 m away from the EMS tower in a mature hemlock stand. The CO_2 uptake by conifer species in 2011 was found to be greatest in April, May, and June (2.1–2.4 g C per m^2 per d) before being drastically reduced in July (0.5 g C per m^2 per d), recovering in August (1.5 g C per m^2 per d) and reducing in the fall (0.4–0.6 g C per m^2 per d; September–October). The conifer uptake flux increased again in November (1.1 g C per m^2 per d) with higher air temperatures before essentially stopping in December (0.008 g C per m^2 per d).

Sap Flow Measurements. Ecosystem-scale flux observations cannot distinguish the canopy flux from the soil flux, because both sinks are located beneath the flux measurement point. Measurements of sap flow through trees (i.e., water uptake by trees) provide understanding of whole-tree transpiration with high temporal resolution when measured continuously throughout the growing season. Because both transpiration and photosynthesis are controlled by stomatal conductance, measurements of sap flow and eddy flux can be combined to understand patterns of canopy carbon uptake (59). We measured rates of sap flow (60) in the dominant (by mass) deciduous tree species [*Quercus rubra* (northern red oak) and *Acer rubrum* (red maple)] in a nearby site at Harvard Forest during a period that overlapped with OCS flux measurements (Figs. S3 and S7). These measurements provide an indication of tree activity that has been used to understand the observed OCS (and CO_2) fluxes. Two sensors were installed at breast height on six individual red oak red maple trees (24 sensors total).

Sap flow rates in both species began to increase on May 19, just after bud break. Senescence began around late October, with water uptake by the red oak continuing until about November 13. Elevated sap flow was generally observed before midnight throughout the growing season before reducing to minimal levels in the early hours of the morning. Fig. S7 shows the summer sap flow rates staying high into the late afternoon after both PAR and the water vapor flux began to decrease. The bulk tree activity, as observed by sap flow rates, showed that the red oaks continued to be active for up to 5 h into the night before reaching zero.

OCS:CO_2 Atmospheric and Ecosystem Relative Uptake

The effect of vegetative uptake on ambient OCS mixing ratios can be explored by looking at a ratio of OCS to CO_2. The atmospheric relative uptake (ARU) is the seasonal change in the OCS:CO_2 uptake ratio (1):

$$\mathrm{ARU} = \frac{[\mathrm{OCS}]_{\mathrm{max-min}}}{[\mathrm{OCS}]_{\mathrm{annual\_mean}}} \times \frac{[\mathrm{CO_2}]_{\mathrm{annual\_mean}}}{[\mathrm{CO_2}]_{\mathrm{max-min}}}, \qquad \mathbf{S4}$$

where $[X]_{\mathrm{max\text{-}min}}$ is the difference between spring maximum and autumn minimum ambient mixing ratios of OCS and CO_2 normalized by their annual mean. We calculate an ARU of 8.5 for 2011, which is similar to the ARU (~8 ± 2) calculated from a multiannual analysis of flask data collected at Harvard Forest for 2000–2005 (1).

The ratio of the ecosystem flux per molecule of OCS to the flux per molecule of CO_2 (f_{OCS}:f_{CO2}) can also be compared with the ecosystem relative uptake (ERU) of OCS to CO_2, reported for studies on larger scales (1, 13). The ERU calculated from aircraft profile data [4.6–6.5 for the New England area in July–August 2004 (13)], was higher than the f_{OCS}:f_{CO2} ratio calculated for the Harvard Forest flux tower in this study: during summer months when photosynthesis was greatest (June–September, excluding July), the mean daily f_{OCS}:f_{CO2} ratio was 2.6 ± 0.7, and the mean daytime (PAR > 300 $\mu E \cdot m^{-2} \cdot s^{-1}$) f_{OCS}:f_{CO2} ratio was 1.5 ± 0.3. The f_{OCS}:f_{CO2} ratio increased from August through October (Table S1). This difference between the aircraft (regional scale) and the tower (local scale) is likely due to the larger nonvegetative sources of CO_2 (including anthropogenic) than OCS (marine and anthropogenic) in the wider region not present within the tower footprint. This example illustrates the value of F_{OCS} data for interpretation of large scale CO_2 signals.

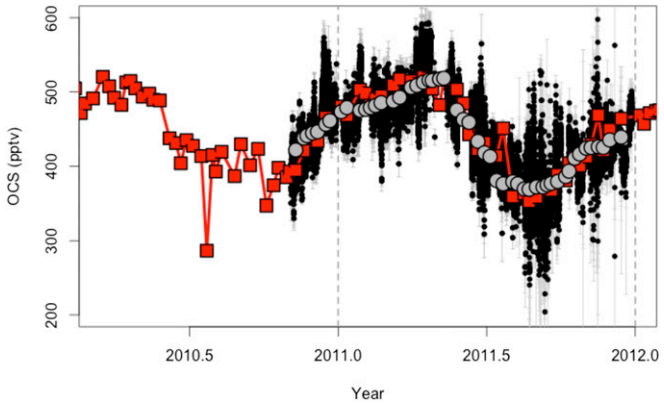

Fig. S1. Comparison of OCS (pptv; pmol·mol^{-1}) measured by the TILDAS [30-min average (black) with 1σ SDs shown in gray], NOAA flask pair means [red points; 1σ SDs shown as red line error bars (barely visible)], and cosampled TILDAS OCS [3-h average at the time of the flask sample (gray circles)]. The flasks were sampled weekly followed by analysis by GC-MS in Boulder as part of the NOAA flask sample network (1).

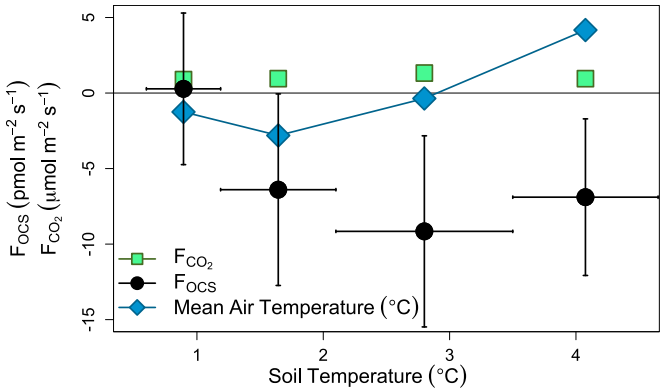

Fig. S2. The OCS (black circles; pmol·m^{-2}·s^{-1}) flux, CO_2 flux (green squares; μmol·m^{-2}·s^{-1}), and the air temperature (blue diamonds; °C) for given surface soil temperatures in December 2011. The data are partitioned to have equal numbers of data points for each temperature shown.

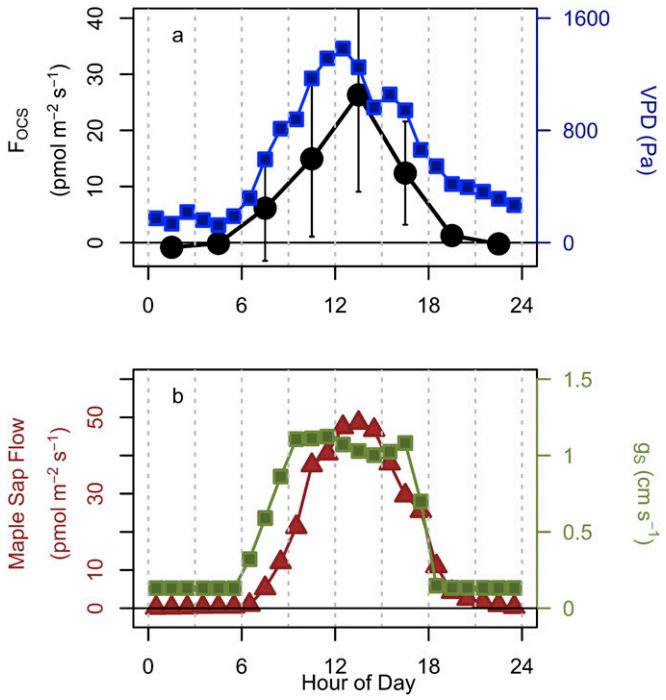

Fig. S3. Diel cycles of (*A*) F_{OCS} (black circles; pmol·m^{-2}·s^{-1}) and VPD (blue squares; Pa) and (*B*) bulk sap flow rate for maple trees (brown triangles; gH_2O·m^{-2}·s^{-1}) and stomatal conductance (g_S; green squares; cm·s^{-1}) for the anomalous OCS emission period on July 19–31, 2011.

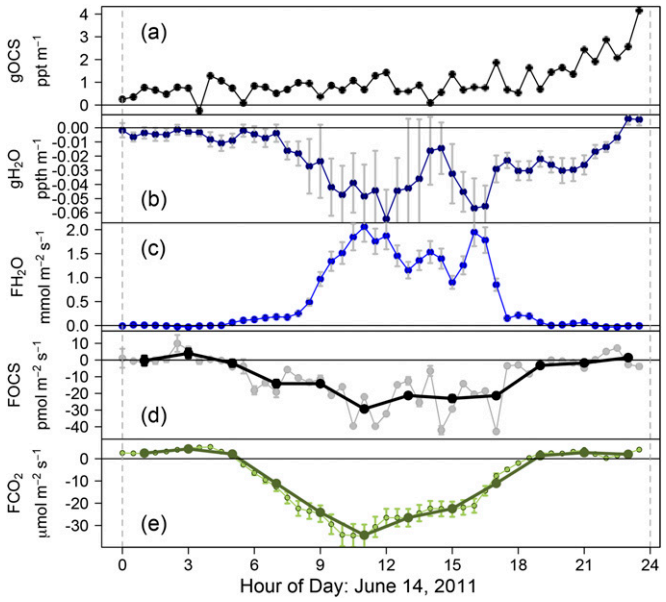

Fig. S4. Components of gradient flux calculated OCS flux for June 14, 2011. (*A*) gOCS: OCS gradient (black; pptv·m^{-1}), confidence intervals of the OCS gradient (gray bars, which are barely visible). (*B*) gH_2O: H_2O gradient (dark blue; pptv·m^{-1}), confidence intervals of H_2O gradient (gray bars). (*C*) FH_2O: H_2O flux (blue; mmol·m^{-2}·s^{-1}), 15% error on eddy covariance measurements (gray bars). (*D*) gFOCS: OCS gradient flux (pmol·m^{-2}·s^{-1}), 2-h average (black), and 30-min gFOCS (gray points with SE as gray bars). (*E*) FCO_2: CO_2 flux (as NEE including storage contribution) (µmol·m^{-2}·s^{-1}), 30-min FCO_2 (small light green points), 15% error on eddy covariance measurements (green bars), 2-h mean (dark green points).

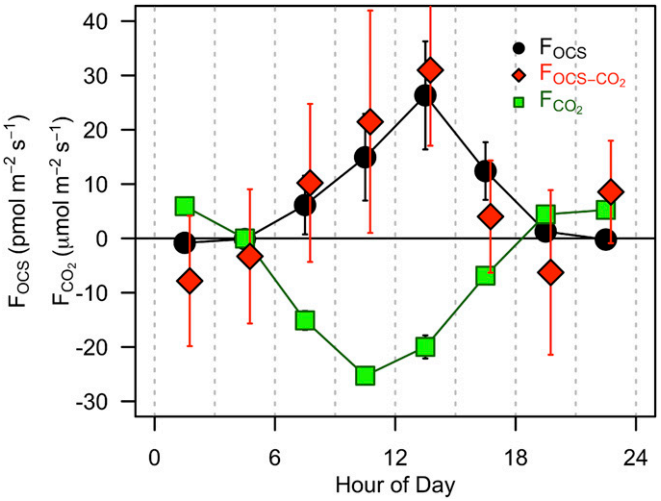

Fig. S5. Composite diel cycle of the gradient flux OCS derived from gradients of water vapor ($F_{OCS.H2O}$; black points) and carbon dioxide ($F_{OCS.CO2}$; red squares) for coincident data in 3 hourly time bins for July 19–31, 2011. The error bars indicate the 95% confidence intervals of the data within the composite 3-h period.

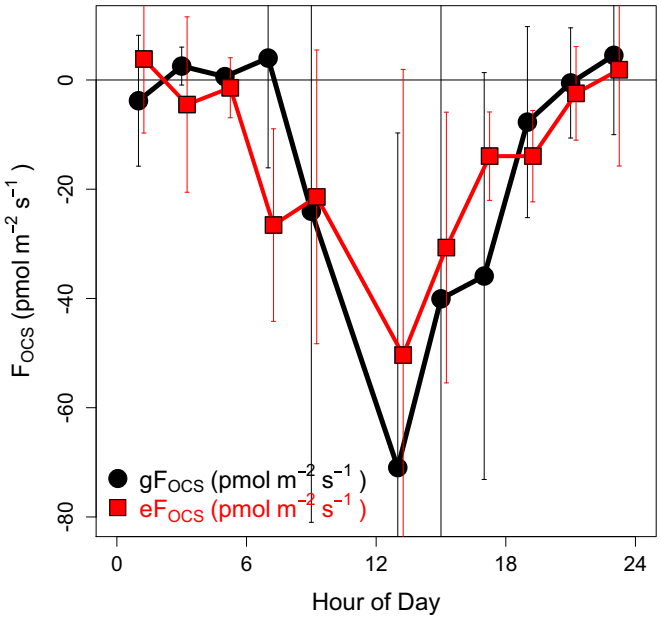

Fig. S6. Composite diel cycle of the gradient flux OCS (gF_{OCS}; black points) and eddy covariance OCS flux (eF_{OCS}; red squares) for coincident data in 2 hourly time bins for August 6–12, 2011. The error bars indicate the 95% confidence intervals of the data within the composite 2-h period.

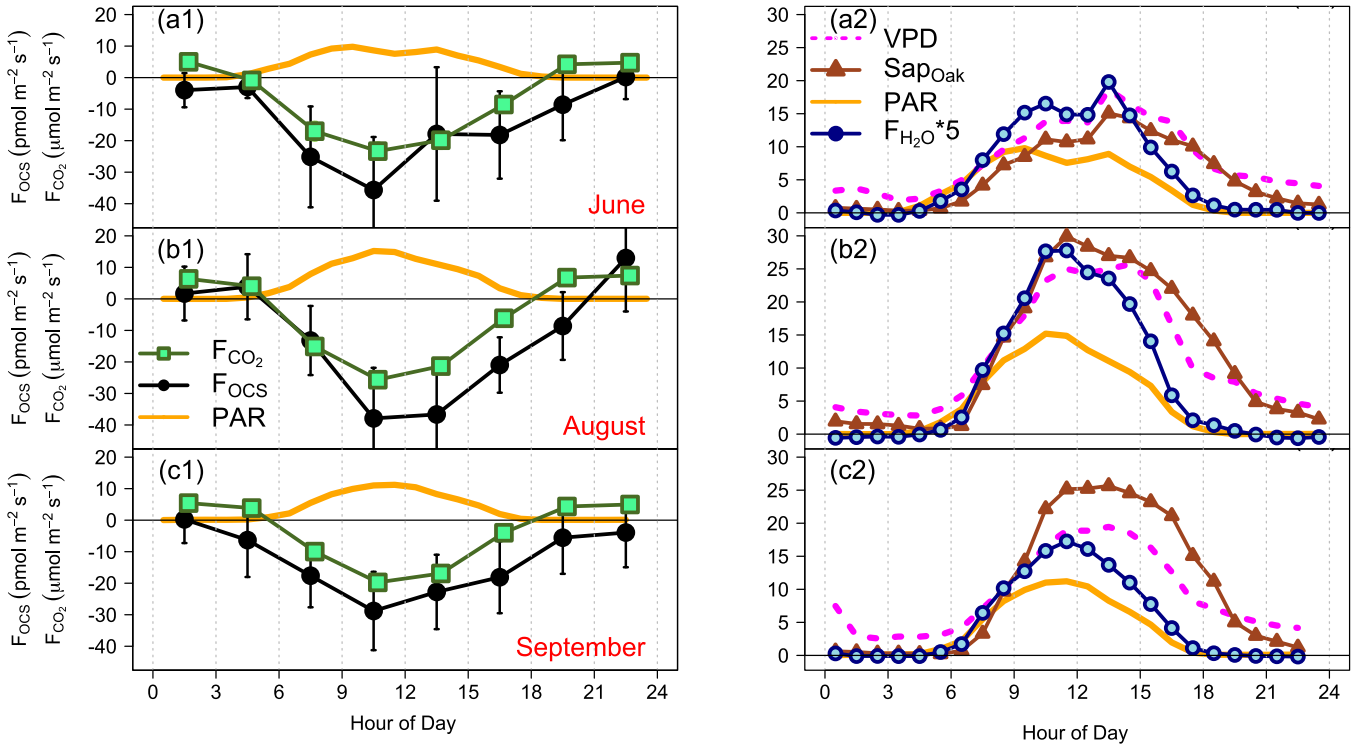

Fig. S7. Diurnal composite of OCS (black) and CO_2 (green) fluxes (Eastern Standard Time) for the summer months of 2011: (*A1*) June, (*B1*) August, and (*C1*) September, with times of low turbulence ($u^* < 0.17$ m·s^{-1}) removed. The 95% confidence intervals for each species are shown as black error bars. The 95% confidence intervals for CO_2 are barely visible. Both columns show PAR (solid orange line; 10^{-8} E·m^{-2}·s^{-1}) on two different scales. *A2*, *B2*, and *C2* show the sap flow rates for oak (brown triangles; gH_2O·m^{-2}·s^{-1}), the vapor pressure deficit (magenta dashed line; Pa), and the water vapor flux [blue/navy circles; 5 mmol·m^{-2}·s^{-1} (multiplied by 5 for graphing)] for June, August, and September.

Table S1. Monthly mean normalized flux

Normalized flux	April	May	June	July	August	September	October	November	December	Year mean
f_{OCS}, m s^{-1}	−0.4	−0.7	−1.3	0.7	−1.6	−1.7	−0.8	−0.5	−0.4	−0.9
f_{OCS}, mmol m^{-2} s^{-1}	−9	−17	−31	18	−39	−43	−18	−10	−10	−22
f_{OCS}/f_{CO2} (ERU)		−0.4	0.7	−2.0	0.8	2.4	3.7	−9.6	5.2	1.4*
f_{OCS}/f_{GEP} (LRU)		1.5	0.5	−0.4	1.2	1.2	0.7	6.6	9.4	1.0*

Monthly mean of ecosystem flux per molecule of OCS (f_{OCS}, m·s^{-1}); ecosystem flux per mole of OCS (f_{OCS}, mmol·m^{-2}·s^{-1}); ratio of the flux per molecule of OCS to that of CO_2 (f_{OCS}/f_{CO2}), comparable to the ERU; and ratio of the flux per molecule of OCS to that of GEP (f_{OCS}/f_{GEP}), comparable to the LRU for daylight hours (PAR > 300 μE·m^{-2}·s^{-1}). Note: Period of net OCS emission in July. This has been removed from the mean year calculation.

*Only the growing season mean (June–October 2011, excluding July) was calculated for f_{OCS}/f_{CO2} and f_{OCS}/f_{GEP} instead of an annual mean. Only data with $u^* > 0.17$ m·s^{-1} have been used in the calculations.